ACS APPLIED POLYMER MATERIALS

pubs.acs.org/acsapm Article

Imprinted Particles for Direct Fluorescence Detection of Sialic Acid in Polar Media and on Cancer Cells with Enhanced Control of Nonspecific Binding

Martha Kimani, Sarah Beyer, Zahra El-Schich, Kornelia Gawlitza,* Anette Gjörloff-Wingren,* and Knut Rurack

Cite This: https://doi.org/10.1021/acsapm.0c01353 Read Online

ACCESS | Metrics & More | Article Recommendations | Supporting Information

ABSTRACT: Glycoproteins are abundant on the cell surface of mammals, providing structural support, modulating cell membrane properties, and acting as signaling agents. Variation of glycosylation patterns has been found to indicate various disease states, including cell malignancy. Sialic acid (SA) is present as a terminating group on cell-surface glycans, and its overexpression has been linked to several types of cancer. Detection of SA on the cell surface is therefore critical for detection of cancer in its early stages. In this work, a fluorescent molecularly imprinted polymer layer targeting SA was synthesized on the surface of silica-coated polystyrene (PS) particles. Compared to previous works, a PS core supplies a lighter, lower-density support for improved suspension stability and scattering properties. Moreover, their smaller size provides a higher surface-area-to-volume ratio for binding. The incorporation of a fluorescent monomer in the MIP shell allowed for simple and rapid determination of binding specificity in polar media due to a deprotonation−reprotonation interaction mechanism between the fluorescent monomer and SA, which led to spectral changes. Upon titration of the MIP particles with SA in suspension, an increase in fluorescence emission of the particles was observed, with the MIP particles binding SA more selectively compared to the nonimprinted polymer (NIP) control particles. In cell staining experiments performed by flow cytometry, the binding behavior of the MIP particles compared favorably with that of SA-binding lectins. NIPs prepared with a "dummy" template served as a better negative control in cell binding assays due to the favorable inward orientation of template-binding functional groups in the polymer shell, which reduced nonspecific binding. The results show that fluorescent MIPs targeting SA are a promising tool for *in vitro* fluorescence staining of cancerous cells and for future diagnosis of cancer at early stages.

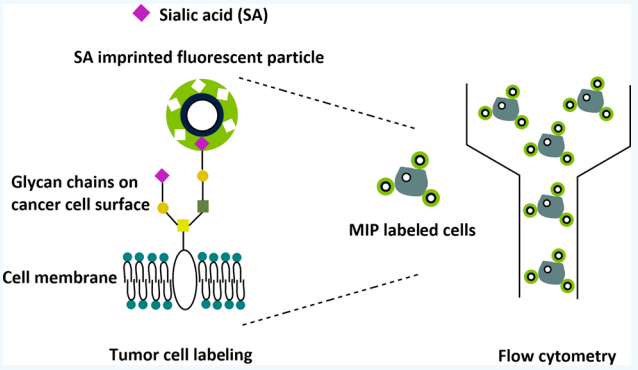

KEYWORDS: *Sialic acid, fluorescence, molecularly imprinted polymers, cancer cells, flow cytometry*

INTRODUCTION

Glycoproteins or glycans are abundant on the cell surface of mammals, providing structural support, modulating cell membrane properties, and acting as signaling agents.[1,2] Variation of glycosylation patterns has been found to indicate various disease states,[3] including cell malignancy.[4] Sialic acid (SA) is present as a terminating group on cell-surface glycans, and its overexpression has been linked to cancer of the prostate, lungs, ovaries, breast, colon, and pancreas.[3] Detection and quantification of SA on the cell surface is therefore critical for detection of cancer in its early stages.

Molecular imprinting techniques for SA detection have gained momentum in the last 20 years. In the earliest reports, Kugimiya et al.[5] and Piletsky et al.[6] imprinted SA in bulk polymers for detection of SA in solution. However, a large proportion of the cavities produced during bulk imprinting is in the inner structure of the polymer and they are not easily accessible. This can be solved by preparation of a thin imprinted polymer film on a support surface to ensure binding sites are located as close to the polymer surface as possible. This promotes access of the analyte to the binding sites and accelerates binding kinetics. Kugimiya prepared an SA-molecularly imprinted polymer (MIP) layer on a quartz crystal microbalance plate and achieved a limit of detection of 20 nmol in water/pyridine mixtures.[7]

Received: December 7, 2020
Accepted: March 23, 2021

More recently, research has focused on techniques for detection of SA directly on the surface of cancer cells. In this regard, MIP layers targeting SA have been prepared on various types of core particles, with a fluorescent emitter being incorporated in the core or shell to allow cell imaging by flow cytometry and fluorescence microscopy. This approach can potentially allow *in vitro* and *in vivo* imaging of cancer cells in the early stages of tumor development. Typical design approaches employ hydrogen bond donors to interact with polar groups on SA or boronic-acid containing functional monomers, which are known to form cyclic esters with SA.[8] Panagiotopoulou et al. utilized (4-acrylamidophenyl)(amino)-methaniminium acetate as a functional monomer to interact with the carboxylate group of SA and synthesized an SA-MIP layer on the surface of quantum dots. The imprinted particles were applied in fluorescence microscopy experiments to stain SA-expressing cells.[9] Li's group synthesized SA-imprinted fluorescent conjugated polymer nanoparticles[10] and graphitic carbon nitride particles[11] containing boronic acid groups for staining of DU-145, an SA-expressing prostate cancer cell line. Wang et al. modified the surface of fluorescein-doped silica beads with boronic acid groups, and after incubation of the particles with an SA solution for cyclic ester formation, silica imprinting was performed with the resulting MIP particles displaying selective labeling of SA on cancer cells, facilitating their detection by flow cytometry.[12] On the other hand, Shinde et al. synthesized an SA-MIP layer on nonfluorescent silica beads and utilized phenyl boronic acid for cyclic ester formation with SA alongside a fluorescent monomer to facilitate cell labeling[13] and observed binding of the particles to human prostate cancer cell lines and a leukemic cell line by flow cytometry and fluorescence microscopy.[14]

In this work, polystyrene (PS) particles were used as supporting particle cores, which are advantageous due to their tunable size and ease in synthesis. In contrast to Shinde's earlier work employing submicron silica particles,[13] smaller PS particles show a lower tendency to sediment because of their lower density, have better scattering properties due to their higher refractive index, and provide a higher surface-area-to-volume ratio for binding.[15,16] After silica coating and subsequent functionalization steps, a fluorescent MIP layer was synthesized on the particle surface by incorporation of a fluorescent monomer whose fluorescence signal was enhanced upon binding of *N*-acetylneuraminic acid, the dominant form of SA in mammalian cells. Interaction between the fluorescent monomer and SA was achieved in a polar medium, *N*,*N*-dimethylformamide (DMF), via a deprotonation−reprotonation mechanism, which led to spectral fluorescence changes in response to the analyte. As the media employed for polymer synthesis and cell staining are distinctly different, two types of nonimprinted polymer particles (NIPs) were prepared for control purposes to assess the influence of nonspecific binding. One was a conventional NIP prepared according to the same recipe as the MIP only without adding template, while the other was a so-called "dummy" NIP, prepared using a "dummy" template that carries the same functional group decisive for signaling as the target template, yet is simpler in chemical structure. Due to the presence of the fluorescent monomer, the binding specificity of the imprinted and nonimprinted particles could be simply determined by fluorescence titrations. Upon titration of the MIP particles with SA in solution, an increase in fluorescence emission of the particles was observed, with the MIP particles binding SA more selectively compared to the conventional NIP and the "dummy" NIP particles. The particles were utilized for staining of cancer cell lines using flow cytometry. The SA-imprinted MIP particles preferentially bound to SA-expressing cells, displaying binding behavior comparable to that of SA-targeting lectins. The conventional NIP particles displayed high unspecific binding to SA-expressing cells, while the "dummy" NIP particles showed significantly lower binding. This was attributed to the difference in surface properties of the two different types of NIPs, with the "dummy" NIP serving as a better negative control in cell binding assays due to the favorable inward orientation of template-binding functional groups in the polymer shell, which reduced nonspecific binding.

For the first time, we demonstrated that the binding specificity of SA-MIPs could be directly investigated by fluorescence titrations in polar media. In addition, we show here that for cell binding applications of MIPs, nonspecific binding events are best compensated for using a NIP prepared with a "dummy" template rather than conventional NIPs since the surface properties of the "dummy" NIP are more comparable to those of the MIP. Our results show that fluorescent MIPs targeting SA are a promising tool for *in vitro* staining of cancerous cells and for future diagnosis of cancer at early stages.

EXPERIMENTAL SECTION

Materials. All organic solvents were purchased from Sigma-Aldrich, abcr, Merck, and J.T. Baker and used without further purification unless otherwise indicated. 2-Isocyanatoethyl methacrylate, styrene, 2,2′-azobis(2-methylpropionamidine)dihydrochloride (AIBA), (3-aminopropyl)triethoxysilane (APTES), methacrylamide (MAAm), ethylene glycol dimethacrylate (EGDMA), tetraethylorthosilicate (TEOS), ammonia 32% solution, and nitric acid (HNO_3) were obtained from Sigma-Aldrich. Triethylamine (TEA), formic acid, and hydrochloric acid were obtained from AppliChem. Basic alumina was purchased from Acros Organics, *N*-acetylneuraminic acid (SA) from Carl Roth, and ethylchloroformate (ECF) from Fluka. The 2,2′-Azobis(2,4-dimethylvaleronitril) (ABDV) initiator was obtained from Wako Chemicals. 4-Cyano-4-(phenylcarbonothioylthio)pentanoic acid (CPDB) and L-lysine were purchased from abcr. Vinylbenzene boronic acid (VBBA) was obtained from Thermo Fisher Scientific. Milli-Q water was obtained from a Milli-Q ultrapure water purification system (Millipore Synthesis A10). Lactic acid (LA) was obtained from J.T. Baker. 4-Chloro-7-nitrobenzofurazan was obtained from Alfa Aesar.

Cell Culture. The epidermal carcinoma cell line A431 and the pulmonary epithelial carcinoma cell line A549 were obtained from the American Type Culture Collection (ATCC, LGC Standards) and cultured in T75 flasks with 10 mL of culture medium. A549 was cultured in RPMI-1640 medium (Thermo Fisher Scientific), supplemented with 10% fetal bovine serum (FBS, Thermo Fisher Scientific) and 1% penicillin−streptomycin (Thermo Fisher Scientific). A431 was cultured in Eagle's minimum Essential medium (EMEM, Sigma Aldrich), supplemented with 10% FBS, 1% L-glutamine (Thermo Fisher Scientific), and 1% nonessential amino acids (NEAA, Thermo Fisher Scientific). Phosphate-buffered saline (PBS) without calcium/magnesium was purchased from Thermo Fisher Scientific. Trypsin/EDTA solution was obtained from Thermo Fisher Scientific. The biotinylated lectins MAL I from *Maackia amurensis* and SNA from *Sambucus nigra* were purchased from Vector Laboratories and streptavidin-fluorescein isothiocyanate (FITC) from Agilent Technologies.

Synthesis of 2-(3-(4-Nitrobenzo[*c*][1,2,5]oxadiazol-7-yl)-ureido)ethyl Methacrylate (I). Fluorescent monomer **I** was synthesized as described previously with modifications.[17] In brief, 4-chloro-7-nitrobenzo-2,1,3-oxadiazole (1.17 g, 5.8 mmol) was

https://doi.org/10.1021/acsapm.0c01353
ACS Appl. Polym. Mater. XXXX, XXX, XXX−XXX

dissolved in methanol (50 mL). Ammonium hydroxide solution (3.5 mL) was added dropwise to the solution under stirring. The reaction was left for 18 h at room temperature and thereafter acidified with 1 M hydrochloric acid solution to pH 1. The resulting suspension was cooled down with an ice bath and briefly filtered. The precipitate was dissolved in water (50 mL) and neutralized with saturated sodium hydrogen carbonate solution (100 mL). The aqueous phase was extracted with ethyl acetate (3 × 100 mL), while the organic phase was dried over sodium sulphate and filtered. The filtrate was concentrated using a rotary evaporator, and the suspension was treated as previously described. Both solid phases were combined and purified by silica gel column chromatography using dichloromethane/ethyl acetate (1 → 1:1 v/v) as the eluent. The precursor of **I**, 7-nitrobenzo[*c*][1,2,5]oxadiazol-4-amine, was obtained as a brown solid (0.46 g, 44% yield). ^{1}H NMR (400 MHz, $CDCl_3$): δ = 8.48 (d, 1H), 6.41 (d, 1H), 5.66 (br s, 2H).

Then, 0.46 g (2.58 mmol) of this solid was dissolved in acetone (20 mL). 2-Isocyanatoethyl methacrylate (0.47 mL, 3.35 mmol) was added dropwise to the reaction solution under stirring, after which triethylamine (0.4 mL) was added dropwise. The reaction mixture was cooled down with an ice bath and briefly filtered and washed with cold acetone (3 × 5 mL). The product was dried overnight under vacuum. **I** was obtained as a bright-yellow solid (0.27 g, 31% yield). ^{1}H NMR (400 MHz, DMSO-d_6): δ 10.28 (br s, 1H), 8.71 (d, 1H), 8.15 (d, 1H), 7.36 (t, 1H), 6.09 (s, 1H), 5.71 (s, 1H), 4.2 (t, 2H), 3.5 (q, 2H), 1.9 (s, 3H). ^{13}C NMR (400 MHz, DMSO-d_6): δ 166.39, 153.59, 145.25, 143.32, 136.71, 135.67, 127.39, 126.00, 109.30, 63.38, 38.36, 17.92 ppm. UPLCMS-TOF (ES+) *m*/*z*: calcd for $[M - H]^+$, 336.0899; found, 336.0999.

Determination of pK_a of I. Solutions of **I** (38 μM) were prepared by diluting a stock solution of the dye in 10 × 10 mm quartz cells containing 2.5 mL of water−ethanol mixture (1:1 v/v). Aliquots of 0.01−1 M KOH or 0.01−1 M $HClO_4$ (60%) in the solvent mixture were added to the solutions under mechanical stirring, while the pH was constantly monitored with a digital pH meter (pH lab 827, Metrohm) equipped with a glass electrode (Biotrode) and calibrated with standard aqueous solutions of pH 4.00, 7.00, and 9.00 from Metrohm. Absorption spectra were taken after addition of each aliquot. For data analysis, pH values in the solvent mixture were activity-corrected, as detailed in ref 18.

Synthesis of PS Particles. Cationic PS particles were synthesized, as previously described.[19] A total of 8.96 mL of Milli-Q water was added to a screw-capped glass vial with a septum. The solution was stirred for 10 min at 75 °C at 600 rpm while degassing with argon. Meanwhile, the inhibitor was removed from styrene using a column packed with basic alumina. Then, 0.05 mL (0.44 mmol) of inhibitor-free styrene was added to the glass vial using a syringe under argon. The solution was mixed for further 10 min at 75 °C at 600 rpm while degassing with argon. Meanwhile, 6.30 mg of AIBA (0.023 mmol) was dissolved in 1.58 mL of Milli-Q water and degassed for 10 min with argon. Then, 1 mL of AIBA solution was added to the water−styrene mixture using a syringe while still being degassed with argon. The reaction mixture was left at 75 °C for 5 h and stirred at 600 rpm. The resulting suspension was cooled down to room temperature and stored at 4 °C.

Synthesis of Silica-Coated PS Particles (SiO_2@PS). Silica coating was performed as previously described with modifications.[20] A total of 28 mL of the aqueous PS suspension was diluted with 25.2 mL of Milli-Q water, and pH was adjusted to 3 using 280 μL of 1 M HNO_3. The mixture was stirred at 700 rpm for 15 min at 60 °C, and then, 78.4 mg of L-lysine (0.54 mmol) in 280 μL of Milli-Q water was added, followed by addition of 252 μL of TEOS (1.14 mmol). The reaction was stopped after 6 h, and the particles were washed three times with 35 mL of 96% ethanol with 10 min of centrifugation at 12,700 *xg* in between. The particles were then dried overnight at room temperature under vacuum.

APTES Modification of SiO_2@PS. APTES modification was performed as previously reported.[15] A total of 102.8 mg of **SiO_2@PS** was suspended 5 min in 4.4 mL of absolute ethanol, then 2.2 mL of 9:1 water/HCl (37%) was added, and the mixture was sonicated for 10 min. The particles were washed twice with 2.2 mL of absolute ethanol and then resuspended in 2.4 mL absolute ethanol. The suspension was degassed briefly with argon, while 110 μL APTES (0.47 mmol) was added. The particles were heated at 40 °C with stirring at 700 rpm for 24 h. Upon completion of the reaction, the particles (**APTES@SiO_2@PS**) were washed twice with 35 mL of absolute ethanol with 10 min of centrifugation at 12,700 × *g* in between and finally dried overnight at room temperature under vacuum.

RAFT Modification of APTES@SiO_2@PS. According to our previous report,[21] 95.1 mg of **APTES@SiO_2@PS** was weighed, and 136.9 mg of CPDB (0.49 mmol) was dissolved in 10.5 mL of dry THF; 52 μL of ECF (0.55 mmol) and 68.1 μL of TEA (0.49 mmol) were added, and the solution was kept in a liquid nitrogen/acetone bath at −60 °C for 40 min. This mixture was then added to the particles, and after light sonication, the particles were mixed at room temperature in a thermomixer at 1000 rpm for 22 h. The particles were precipitated with 10 mL of hexane and washed twice with 20 mL of THF with 5 min of centrifugation at 12,700*g* in between. The particles (**RAFT@SiO_2@PS**) were dried overnight at room temperature under vacuum.

MIP and NIP Synthesis on RAFT@SiO_2@PS. A total of 5.5 mg of **I** (0.016 mmol), 2.7 mg of MAAm (0.032 mmol), 2.4 mg of VBBA (0.016 mmol), and 123 μL of EGDMA (0.65 mmol) were dissolved in 6 mL of DMF and placed in an ultrasonic bath for 15 min (prepolymerization mixture). Meanwhile, 1.8 mg of SA (0.0058 mmol) and 0.374 μL of LA (0.0058 mmol) were each dissolved in 500 μL of DMF; 20 mg of **RAFT@SiO_2@PS** was weighed in three separate glass vials. To each vial, 2 mL of the prepolymerization mixture was added, followed by addition of 500 μL of either the SA solution (for **MIP@SiO_2@PS**), the LA solution (for the "dummy" **LA-NIP@SiO_2@PS**, explanation see Results and Discussion section), or DMF (for the conventional **NIP@SiO_2@PS**). The particles were suspended 20 min in an ultrasonic bath. Meanwhile, 4.0 mg of ABDV (0.016 mmol) was dissolved in 3.56 mL of DMF and degassed till usage. After sonication, the particles were put to heat at 50 °C and 500 rpm while degassing with argon for 20 min. Then, 600 μL of ABDV solution in DMF was added to each vial and the reaction continued for 22 h. Upon completion of the reaction, 800 μL of MeOH was added to the particles and they were centrifuged at 3500 × *g* for 5 min. The template was removed by mixing the particles with 1.5 mL of cleaning solution (methanol (80.9%), formic acid (14.3%), and Milli-Q water (4.8%)) for 1 h with a thermomixer at RT at 1,000 rpm. The particles were centrifuged at 3220 × *g* for 2 min. This was repeated three times. Thereafter, 1.87 mL of MeOH was added to the particles, and they were placed on a rotating plate at 40 rpm for 30 min. The particles were centrifuged at 10,000 × *g* for 5 min and then dried overnight at room temperature under vacuum.

Cell Binding Studies. A549 and A431 cells were incubated at 37 °C in a 5% CO_2 atmosphere at 100% humidity until they were confluent. For the passage of the cells, the cells were washed with 10 mL of PBS and treated with 700 μL of trypsin/EDTA solution to detach the cells from the flasks. The cells were counted and pelleted in a centrifuge for 5 min at 300 × *g* and then washed with 3 mL of PBS. **MIP@SiO_2@PS**, **NIP@SiO_2@PS**, and **LA-NIP@SiO_2@PS** were added at a concentration of 0.1 mg mL^{-1} to 1 × 10^6 cells in 100 μL of PBS. As a negative control, one sample of cells was left with only 100 μL of PBS. The cell samples were incubated in the dark at 4 °C for 30 min and then washed twice with 1.5 mL of PBS (centrifugation for 5 min at 300*g*). The biotinylated lectins MAL **I** and SNA, respectively, were added at a concentration of 5 μg mL^{-1} to 5 × 10^5 cells in 100 μL of PBS. The samples were incubated in the dark at 4 °C for 30 min and washed twice with 1.5 mL of PBS, followed by staining with 10 μg mL^{-1} streptavidin-conjugated FITC and further incubated in the dark at 4 °C for 20 min. One sample of cells was only stained with 10 μg mL^{-1} streptavidin-conjugated FITC as a negative control. After incubation, the cells were washed twice with 1.5 mL of PBS. Finally, all cell samples were resuspended in 300 μL of PBS for analysis in a flow cytometer. A total of 10,000 gated events were captured for the analysis of the MIP and NIP binding.

https://doi.org/10.1021/acsapm.0c01353
ACS Appl. Polym. Mater. XXXX, XXX, XXX−XXX

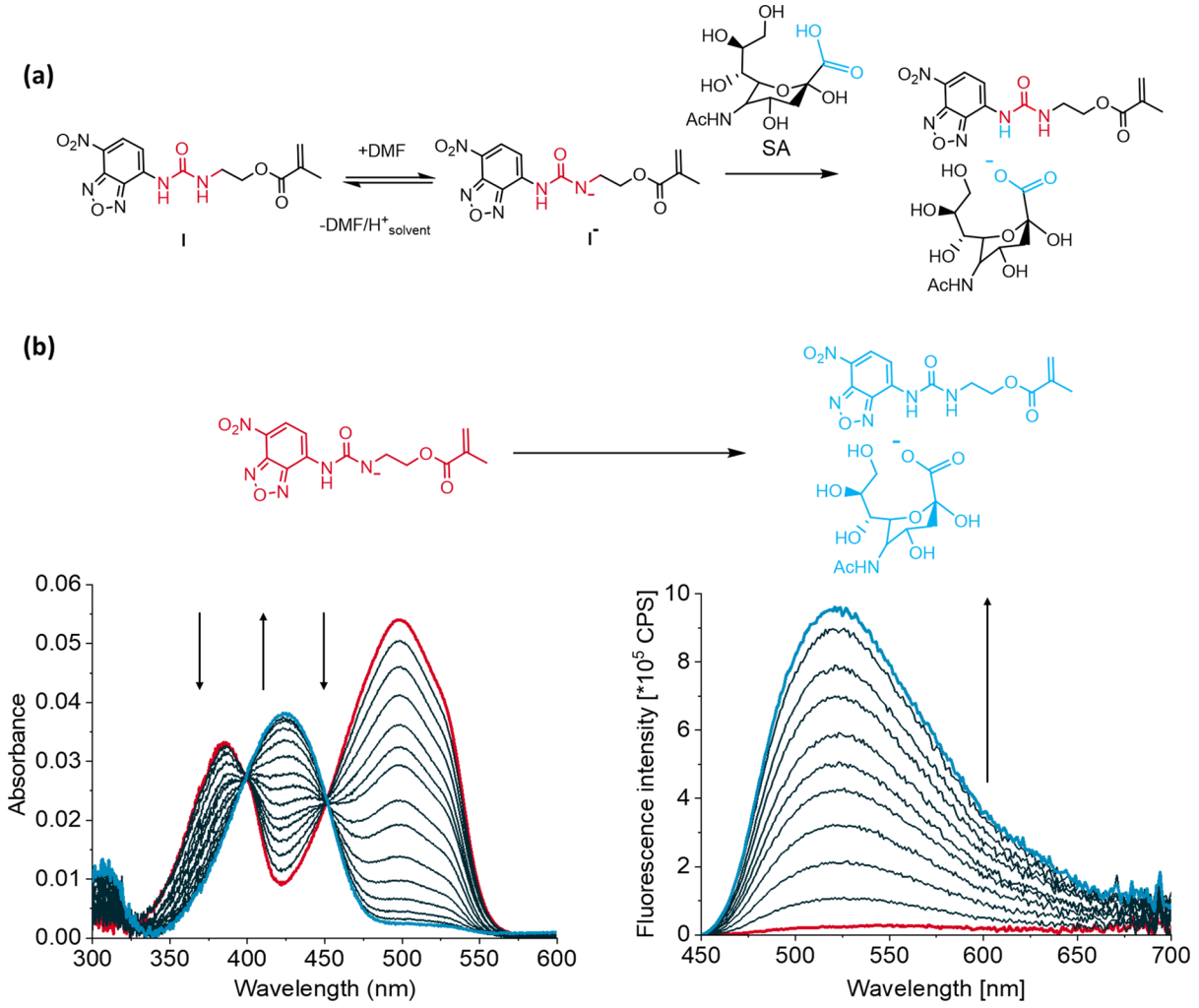

Figure 1. (a) Deprotonation of **I** in DMF and subsequent reprotonation by SA. (b) Absorption (left) and fluorescence (right) spectra (λ_{exc} = 424 nm) of **I** (3 μM) before (red line) and after (blue line) addition of SA (0.71−180 μM) in DMF.

Instrumentation. ^{1}H and ^{13}C NMR spectra were recorded on Bruker AV-400 and AVANCE III 500 spectrometers, mass spectra were obtained on a Waters LCT Premier XE-TOF mass spectrometer, TEM images were registered with a Talos F200S (200 kV) transmission electron microscope (FEI). UV/Vis absorption spectra were recorded on an Analytik Jena Specord 210 Plus spectrophotometer. Steady-state fluorescence measurements were carried out on a Horiba Jobin−Yvon FluoroMax-4P spectrofluorometer. Standard 10 mm path-length quartz cuvettes were used for dye and particle measurements. Dynamic light scattering experiments were performed with a Zetasizer Nano ZS (Malvern Instruments). Infrared spectroscopy (IR) measurements were performed with an Equinox55 spectrometer (Bruker) using a 15× objective lens with the measurement sample on a silica plate. Elemental analysis measurements were performed on an ELTRA CS 800 carbon/sulfur analyzer. Flow cytometry measurements were performed using an AccuriC6 flow cytometer from BD Biosciences.

Particle Characterization. For TEM measurements, 0.04 mg mL^{-1} particle suspensions were prepared in absolute ethanol and 9 μL was placed on a copper grid with a carbon film. Images were analyzed with Image J software (National Institutes of Health and the Laboratory for Optical and Computational Instrumentation).[22] To determine the diameter of the particles, data from 150 particles were collected, and the average and standard deviation of the measurements were calculated. To perform fluorescence titrations, 0.20 mg mL^{-1} suspensions of the **MIP@SiO$_2$@PS**, **NIP@SiO$_2$@PS**, and **LA-NIP@SiO$_2$@PS** particles were prepared in DMF; a 1 mM solution of SA in DMF was also prepared. Increasing volumes of the 1 mM SA solution were added to 2 mL suspensions of the **MIP@SiO$_2$@PS**, **NIP@SiO$_2$@PS**, and **LA-NIP@SiO$_2$@PS** particles, and after 2 min of stirring for each addition step, the resultant absorption and fluorescence spectra were recorded. $\frac{\Delta F}{F_0} = \frac{F_x - F_0}{F_0}$ was calculated for each fluorescence spectrum of the **MIP@SiO$_2$@PS**, **NIP@SiO$_2$@PS**, and **LA-NIP@SiO$_2$@PS** particles (where F_x is the fluorescence intensity at 513 nm for each spectrum after SA addition, while F_0 is the fluorescence intensity at 513 nm before addition of SA). The imprinting factor was determined from the MIP/NIP ratio of $\frac{\Delta F}{F_0}$ at the saturation point of the titration. For zeta potential measurements, 0.04 mg mL^{-1} particle suspensions were prepared in Milli-Q water and measurements performed using disposable folded capillary cells.

RESULTS AND DISCUSSION

Binding of I with SA. Fluorescent probe **I** containing a urea motif (Figure 1) has been reported as a probe monomer for deprotonated anions in chloroform through a hydrogen bonding mechanism, with association constants from 10^3 to 10^5 M^{-1}.[17,23] To utilize **I** as a fluorescent reporter in polar solvents used in cell experiments, Shinde et al. incorporated **I** in MIP particles targeting SA in methanol/water mixtures. However, the binding ability of **I** to SA was low as determined from the weak fluorescence changes observed upon addition of

https://doi.org/10.1021/acsapm.0c01353
ACS Appl. Polym. Mater. XXXX, XXX, XXX−XXX

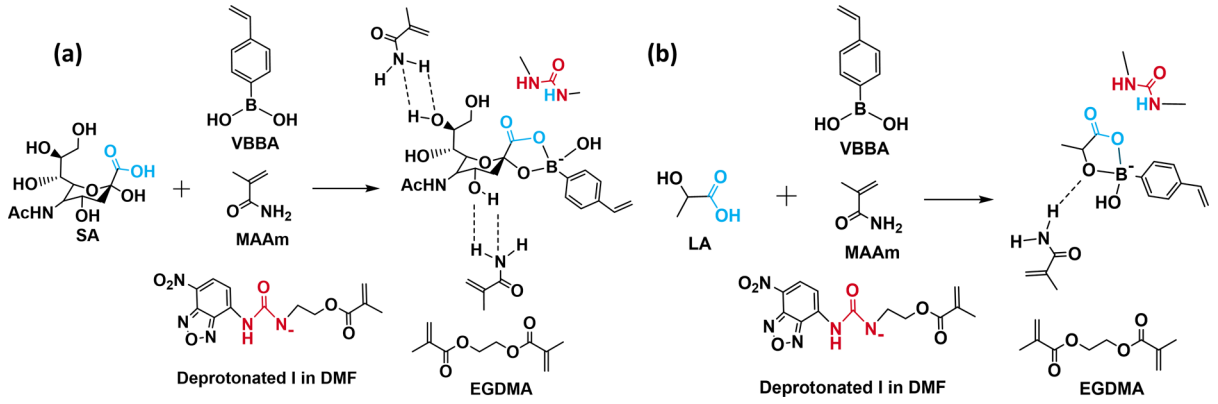

Figure 2. Functional monomers and the cross-linker used in **MIP@SiO$_2$@PS** (a) and **LA-NIP@SiO$_2$@PS** (b) synthesis and their interactions with the corresponding template in DMF.

SA owing to the disruption of hydrogen bonds by the polar solvents used.[13] For strong interaction to occur between **I** and SA in polar media, alternative modes are thus required.

DMF, a polar aprotic solvent, has been previously used as a solvent medium for synthesis of nonfluorescent MIPs targeting SA, with satisfactory binding being obtained thereafter in water/organic solvent mixtures[7] and aqueous buffers.[5,6] Therefore, it was expected that fluorescent MIP particles synthesized in DMF could be used as well for SA labeling of cells in physiological buffers. The spectroscopic behavior of the fluorescent monomer **I** was therefore investigated in dilute solution in DMF. **I**, whose pK_a was determined to be 8.1 ± 0.1, was observed to undergo deprotonation under these conditions due to the basic character of the solvent.[24,25] Absorption spectra of $\mathbf{I}^-$ in DMF show deprotonation bands at 385 nm and at 498 nm, but the deprotonated species $\mathbf{I}^-$ is only weakly fluorescent upon excitation at 424 nm. After addition of SA, a new absorption band is formed at 424 nm, accompanied by an increase in fluorescence emission at 524 nm (Figure 1a,b; see Figure S3 in the Supporting Information). This indicated that the carboxylic acid group of SA reprotonates $\mathbf{I}^-$ to its neutral form. The fluorescence quantum yield (Φ_f) of the two different forms of **I**, neutral and anionic, obtained following excitation at 424 nm and at 498 nm were determined to be 0.125 ± 0.004 and 0.004 ± 0.002, respectively (see the Supporting Information for further details). Because $\mathbf{I}^-$ is only very weakly emissive, its fluorescence has no analytical relevance for cell imaging or SA sensing in aqueous media and was thus not further considered in this work. The protonation of $\mathbf{I}^-$ by SA fits a 1:1 binding model, yielding an apparent reprotonation constant of K_a^{abs} = 6.6 (±0.6) × 10^4 M^{-1} at 24 °C (see the Supporting Information for details).[26] Analysis of the corresponding fluorescence data yielded a K_a^{fluo} = 7.2 (±1.0) × 10^4 M^{-1}. The certain deviation of these data and the associated uncertainties are most likely due to the fact that the two processes immanent to Figure 1a, reprotonation of $\mathbf{I}^-$ by SA and (loose) hydrogen bonding between **I** and SA^-, cannot be easily distinguished spectroscopically. However, as this behavior would be even beneficial in terms of molecular recognition, **I** could be used as a functional monomer in the synthesis of fluorescent MIP particles for the formation of SA-specific binding cavities, allowing for determination of binding behavior directly through fluorescence titrations in DMF. Thereafter, the SA-imprinted particles could be used in cell staining experiments in aqueous buffer, with **I** acting as the fluorescent reporter for particles bound to cells.

MIP Recipe Optimization. For successful MIP formation, strong interactions between the template molecule and the resulting polymer matrix should occur. This requires careful selection of comonomers used in the synthesis and a suitable cross-linker for the formation of a polymer shell with highly specific binding cavities. The choice of comonomers and cross-linkers depends on the functional groups present on the template and the desired properties of the resulting particles.

SA is a sugar acid derivative containing several hydroxyl groups, an acetylated amino group, and an α-hydroxy carboxylic acid group. Boronic acid groups are known to form cyclic esters with the diols of sugars.[8] However, SA has been reported to preferentially interact with phenyl boronic acids via the α-hydroxy carboxylic acid group to form a tetrahedral anionic ester, even when the carboxylic acid is deprotonated.[27] In order to perform stoichiometric imprinting so that binding of the template to as many cavities as possible resulted in a measurable fluorescence response, $\mathbf{I}^-$ in DMF was used as the primary sensing group for SA with vinyl benzene boronic acid (VBBA) chosen as an additional functional monomer to further aid in SA interaction. The α-hydroxy carboxylate group of SA generated by protonation of $\mathbf{I}^-$ in DMF was expected to form a tetrahedral cyclic ester with VBBA. Methacrylamide (MAAm) was chosen as comonomer as it can further stabilize hydrogen-bonded ensembles, as shown in Figure 2a, presumably promoting the ability of SA to reprotonate $\mathbf{I}^-$. EGDMA is readily available and commonly used as a cross-linker in MIP synthesis to form a polar matrix (Figure 2a).[28] Alongside **I**, the chosen comonomers facilitate strong interaction with SA to allow for formation of highly specific binding cavities in the resulting MIP layer.

In order to account for nonspecific interactions, control nonimprinted particles (**NIP@SiO$_2$@PS**) were prepared. In addition to conventional NIPs without the template, "dummy" NIPs (**LA-NIP@SiO$_2$@PS**) using lactic acid (LA) as a "dummy" template were also prepared to ensure that the formation of the polymer shell and the resulting polymer properties in the MIP and NIP are similar. LA is an α-hydroxy carboxylic acid like SA, and it has been reported that the lactate anion forms a tetrahedral anionic ester with boronic acids in the same way as deprotonated SA.[29] Therefore, LA is expected to interact with the functional monomers in a manner similar to SA (Figure 2b). Moreover, inclusion of a "dummy" template in the NIP ensures that the functional monomers are favorably oriented in the inner matrix rather than on the surface. This is critical particularly for boronic acid and amide functionalities

https://doi.org/10.1021/acsapm.0c01353
ACS Appl. Polym. Mater. XXXX, XXX, XXX−XXX

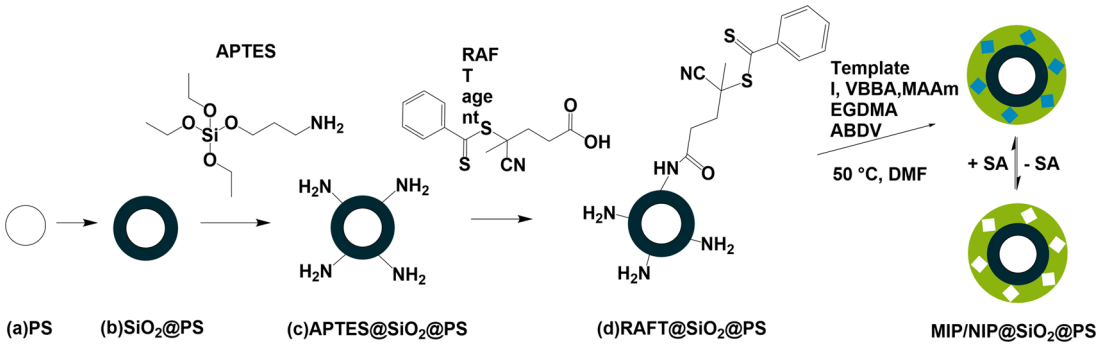

Figure 3. Synthesis scheme of MIP particles on a PS core.

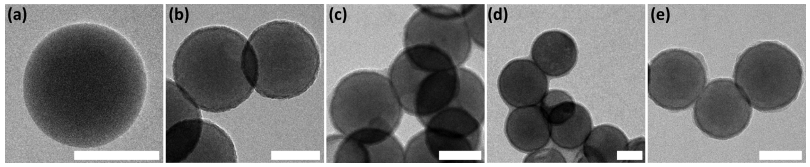

Figure 4. TEM images of (a) PS, (b) **SiO_2@PS**, (c) **MIP@SiO_2@PS**, (d) **NIP@SiO_2@PS**, and (e) **LA-NIP@SiO_2@PS**. Scale bar = 100 nm.

whose presence on the NIP surface is expected to increase nonspecific binding events in cell binding studies due to interactions with nontarget groups on the cell surface.[3] Therefore, binding cavities specific to LA rather than SA were introduced into the **LA-NIP@SiO_2@PS**. The appropriate component ratio for MIP synthesis was determined to be template/**I**:VBBA/MAAm:EGDMA = 1:1:1:2:40 from a previous work.[13]

Synthesis and Characterization of MIP and NIP Particles. PS nanoparticles were utilized as supports for MIP synthesis due to ease of synthesis and control of particle size.[19,30] In contrast to Shinde's earlier work employing submicron silica particles,[13] smaller PS particles show a lower tendency to sediment due to their lower density and have better scattering properties because of the higher refractive index, as well as provide a higher surface-area-to-volume ratio for binding. Synthesis of a thin polymer shell on the particle surface would allow easy access of SA on cells to the corresponding binding sites on the particle surface. To facilitate this process, reversible-addition fragmentation chain transfer (RAFT) polymerization was used.

First, cationic PS particles (diameter from TEM 168.9 ± 19.3 nm) were synthesized according to previously reported protocols.[19,20] Silica coating of the particles was then performed to protect the PS core from swelling by DMF during MIP synthesis and allow functionalization of the particle surface. The silica surface was modified by functionalization with amino groups through the reaction with APTES, followed by condensation of the amino groups with the carboxylic acid group of a RAFT agent, 4-cyano-4-(phenylcarbonothioylthio)pentanoic acid.[21,31] The amount of RAFT groups immobilized on the surface was determined by elemental analysis of sulfur, which is only present in the dithiophenyl group of the RAFT agent in the respective hybrid material. The particles contained 0.364% sulfur by weight, corresponding to 0.0568 mmol g^{-1} of RAFT groups. After RAFT functionalization of the silica surface, MIP synthesis was performed on the particle surface using the polymerization recipe outlined above (Figure 3), and the particles were thereafter washed three times for removal of templates from **MIP@SiO_2@PS. LA-NIP@SiO_2@PS** and **NIP@SiO_2@PS** were washed in the same way for comparability. Normalized absorption spectra of the washed particles revealed overlap of the spectra of **MIP@SiO_2@PS**, **LA-NIP@SiO_2@PS**, and **NIP@SiO_2@PS**, showing that template removal was successful (see Figure S5 in the Supporting Information).

The different synthesis and functionalization steps of PS core/silica shell particles led to changes in the particle surface properties, as revealed by zeta potential measurements (see Figure S6 in the Supporting Information). Cationic PS possessed a net positive charge due to the presence of amino groups from the cationic initiator used. Silica coating resulted in a change to a negative potential due to introduction of silanol groups, and after APTES modification, the zeta potential became more positive with the introduction of amino groups on the surface. Coupling of the RAFT reagent to some of the amino groups on the particle surface reduced the net positive charge from the APTES groups. IR spectra also revealed successful functionalization of the particles (see Figure S7 in the Supporting Information).

From TEM images (Figure 4), a uniformly sized silica shell (7.9 ± 1.0 nm) was formed on the cationic PS. Polymer shell formation was also observed due to the presence of an organic material on the outer surface of the silica shell in MIP and NIP particles. The polymer shell thickness was determined from statistical analysis of TEM images. For **MIP@SiO_2@PS**, the polymer shell was 9.0 ± 2.8 nm, for **NIP@SiO_2@PS**, 9.7 ± 2.6 nm, and for **LA-NIP@SiO_2@PS**, 7.7 ± 2.4 nm.

Fluorescence Titrations of Particles. In many cases, the binding capacity of MIPs is determined from incubation of the imprinted particles with the template solution, followed by quantification of the unbound template in the supernatant, which is then used to calculate the amount of the bound template. This is a time-consuming process, which increases the uncertainty of the measurement from the several steps involved. Moreover, the analyte concentration in the binding solution may be reduced by processes other than MIP binding, such as adhesion to glassware or degradation. In this work, the incorporation of fluorescent monomer **I** allowed the direct

https://doi.org/10.1021/acsapm.0c01353
ACS Appl. Polym. Mater. XXXX, XXX, XXX−XXX

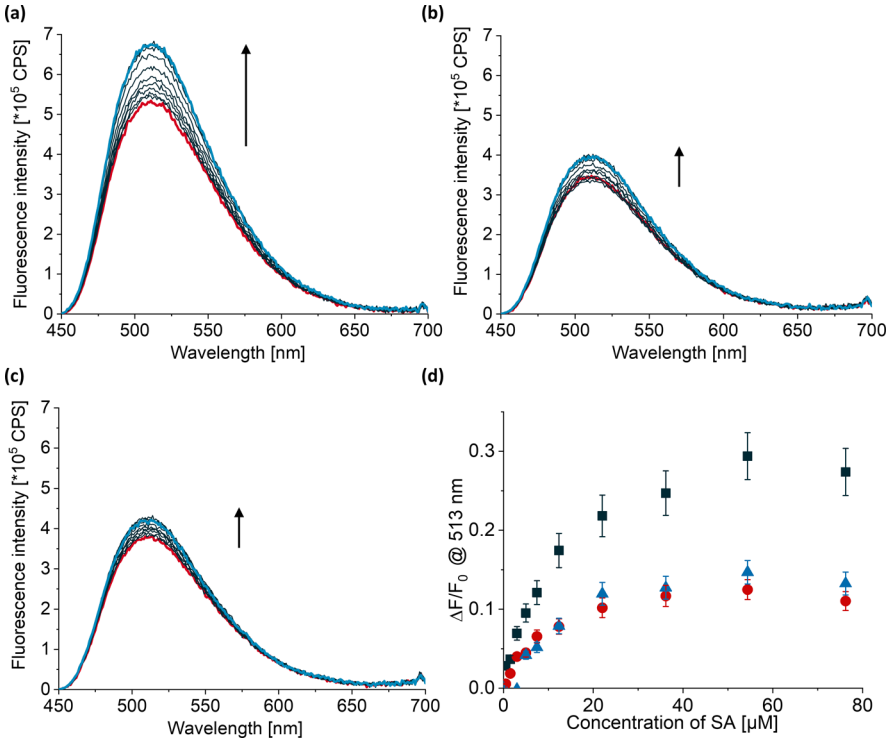

Figure 5. Fluorescence emission spectra (λ_{exc} = 424 nm) of (a) **MIP@SiO$_2$@PS**, (b) **NIP@SiO$_2$@PS**, and (c) **LA-NIP@SiO$_2$@PS** in DMF before (red) and after (blue) addition of up to 76 μM SA in DMF. (d) Comparison of the fluorescence response of **MIP@SiO$_2$@PS** (black squares), **NIP@SiO$_2$@PS** (blue triangles), and **LA-NIP@SiO$_2$@PS** (red circles). $\frac{\Delta F}{F_0} = \frac{F_x - F_0}{F_0}$, where F_x is the fluorescence intensity at 513 nm for each spectrum after SA addition, while F_0 is the fluorescence intensity at 513 nm before addition of SA. The imprinting factor was determined from the MIP/NIP ratio of $\frac{\Delta F}{F_0}$ at the saturation point of the titration.

determination of binding specificity of the particles by fluorescence titrations with SA in DMF solution.

Upon suspension of the particles in DMF, deprotonation of **I** in the particles was observed in absorption spectra through the presence of a band at ca. 500 nm. Upon addition of SA, the band at 500 nm decreased in intensity until saturation was reached after addition of 76 μM SA to the particle suspension. The band of charge-neutral **I** observed at 424 nm in solution shifted to 433 nm in the synthesized particles, and the absorbance at this band increased upon addition of SA to the particles (see Figure S8 in the Supporting Information), accompanied by a fluorescence increase at 513 nm (λ_{ex} = 424 nm) (Figure 5). The fluorescence quantum yield Φ_f of the neutral form of **I** was determined to be 0.047 ± 0.004 (see the Supporting Information for further details). The slightly lower Φ_f in the polymer shell compared to neat DMF is presumably due to the fact that **I** is confined in a somewhat less polar microenvironment, as supported by a blue-shifted emission maximum of 513 nm in the shell (vs 524 nm in solution). A reduction in local polarity is known to reduce the fluorescence yield of NBD dyes.[17] Due to the formation of specific binding cavities in **MIP@SiO$_2$@PS** compared to **NIP@SiO$_2$@PS** and **LA-NIP@SiO$_2$@PS**, the fluorescence increase observed for **MIP@SiO$_2$@PS** was higher than that observed with either of the NIPs (Figure 5). Moreover, the apparent reprotonation/interaction constant K_a^{fluo} was determined to be 8.87 (±1.21) × 10^4 M^{-1} for **MIP@SiO$_2$@PS** and SA from the data in Figure 5a, which is higher than that for **I** in DMF, hinting at the successful formation of cavities in the MIP shell. The response time of the MIPs and NIPs was measured in kinetic experiments and revealed that SA penetration to the binding sites occurred instantaneously, at least within the limit of the experiment (<10 s), which was consistent with the thin polymer shells observed from TEM measurements (see Figure S9 in the Supporting Information).[17] The fluorescence response of the MIP particles remains virtually unchanged within experimental uncertainty, and the particles were used over a 1 year period with consistent results. By comparing the relative fluorescence response, the imprinting factors for **MIP@SiO$_2$@PS** against **NIP@SiO$_2$@PS** and **LA-NIP@SiO$_2$@PS** were determined to be 2.00 and 2.35 respectively. As expected, the use of a "dummy" template reduced the nonspecific binding events compared to NIPs prepared without the template. In suspension, the fluorometric analytical figures of merit, limits of blank, detection, and quantification (LOB, LOD, and LOQ), were calculated to be 2.1, 2.9, and 3.2 μM, respectively (see the Supporting Information for details). Increased levels of SA in saliva have been reported in breast cancer patients[32] at levels of up to 5.82 μM.[33] The **MIP@SiO$_2$@PS** particle probes could thus be employed to quantify SA directly in such environments following an extraction step.

The cross-selectivity of **MIP@SiO$_2$@PS** was investigated against other sugar derivatives that would be in close proximity to SA groups on the tumor cell surface. *N*-Acetylgalactosamine (GalNAc) is present in the Tn motif to which SA groups are usually attached in cancer cells,[3] while glucose is present in cell culture media as an energy substrate for dividing cells. Titration of **MIP@SiO$_2$@PS** with GalNAc and glucose did not induce a fluorescence increase (see Figure S11, Supporting

https://doi.org/10.1021/acsapm.0c01353
ACS Appl. Polym. Mater. XXXX, XXX, XXX−XXX

Information). After confirming the selectivity of the MIPs in solution, the particles were utilized in cell binding studies.

Cell Binding Studies of MIP and NIP Particles to Cancerous Cell Lines (A549 and A431). The glycan branching pattern of SA varies in different cell types, depending on the protein and lipid distribution on the cell surface.[2] Terminal SA groups are attached to the glycan chains via linkage to other sugar residues such as GalNAc either by α-2,3 or α-2,6 configuration (see Figure 6). α-2,3 SA and α-2,6 SA have a different distribution in some epithelial cell lines.[34]

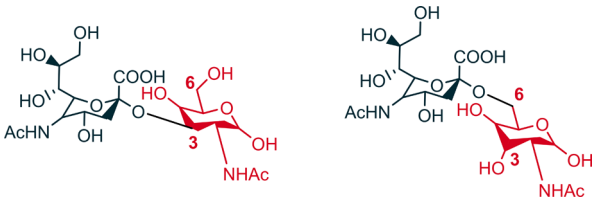

Figure 6. α-2,3 (left) and α-2,6 (right) linkages of SA (black) to GalNAc (red).

To investigate the SA-binding properties of the MIP and NIP particles, two cancer cell lines known to express SA were chosen: the epithelial lung cancer cell line A549 and the epidermal skin carcinoma cell line A431. First, the α-2,3 and α-2,6 SA expression of the two cell lines was validated by lectin binding. This was investigated by flow cytometry using MAL **I** and SNA lectins, which bind preferentially to α-2,3 and α-2,6 SA, respectively. The mean fluorescence intensity (MFI) was used to quantify the binding of lectins to cells. This is because the lectins are small enough to bind individual SA units, and therefore, the total fluorescence emission observed from the bound lectins is proportional to the total amount of SA present on the cell surface. The results showed that A431 cells preferentially express α-2,3 SA, while A549 cells express both α-2,3 and α-2,6 SA (see Figure 7 and Figure S12 in the Supporting Information).

Thereafter, the binding behavior of the MIP and NIP particles to the two cell lines was investigated by flow cytometry. Instead of MFI, the percent of labeled cells was considered to be a more reliable metric for quantification of binding of the particles. The particles are much larger in diameter (ca. 170 nm) than lectins (up to several nanometers), and binding to individual SA molecules on the cell surface is not possible. Moreover, aggregation of the particles can occur in physiological buffers, which would artificially increase the observed MFI. The flow cytometry results are summarized in Figure 8 (see Figures S13 and S14 in the Supporting Information for further details). Interestingly, the binding of **MIP@SiO$_2$@PS** and **NIP@SiO$_2$@PS** to the two cell lines was very similar, resulting in 20−25% labeled cells and 25−30% labeled cells, respectively. On the contrary, **LA-NIP@SiO$_2$@PS** showed only ca. 5% binding to both cell lines, which was significantly lower than **MIP@SiO$_2$@PS** and **NIP@SiO$_2$@PS**.

It is expected that **MIP@SiO$_2$@PS** would bind both α-2,3 and α-2,6 SA on the cell surface since imprinting was performed using only SA, resulting in binding sites without geometrical specificity for either of the two forms. However, α-2,3 and α-2,6 SA are configured differently on the cell surface. α-2,3 SA is apically positioned and is more exposed outwardly on the cell surface compared to α-2,6 SA, which shows a more basolateral localization and is oriented inward on the cell surface, which may lead to a more effective binding of **MIP@SiO$_2$@PS** to α-2,3 SA.[34,35] A similar binding pattern of **MIP@SiO$_2$@PS** to A549 and A431 could point to a preferential binding of the particles to α-2,3 SA since the binding of MAL **I** to both cell lines was comparable. To confirm this hypothesis, we are currently determining the MIP staining pattern of more than 10 cancer cell lines derived from breast, prostate, and white blood cell populations, which will reveal more information and on which we will report separately.

Comparison of Binding Response of Particles in Suspension and in Cell Experiments. The results from rebinding experiments in suspension and from cell binding studies clearly show that **MIP@SiO$_2$@PS** particles bind higher amounts of SA than **LA-NIP@SiO$_2$@PS**, while **NIP@SiO$_2$@PS** show lower binding to SA in suspension but high apparent binding to SA in cell experiments. These differences can be explained by the varying nature of the polymer network of the particles and the different detection mechanisms used in suspension and in flow cytometry. Figure 9 schematically shows the putative distribution of **I**, amide and boronic acid moieties in the polymer layer of the investigated particles. In suspension, the template reprotonates the fluorescent monomer **I**, resulting in a measurable increase in fluorescence emission, which is then used for the evaluation of binding. For **MIP@SiO$_2$@PS** particles, there are specific binding cavities for SA, created by the reprotonation of $\mathbf{I}^-$ by SA, boronic ester formation with VBBA, and hydrogen bonding interactions with MAAm, and therefore, the fluorescence increase observed is higher than with **NIP@SiO$_2$@PS** or **LA-NIP@SiO$_2$@PS**. In the latter, the small fluorescence increases can be attributed to nonspecific interaction between those molecules of **I** that are directly at the surface and SA since no SA-specific cavities are present. In cell binding assays using flow cytometry, however,

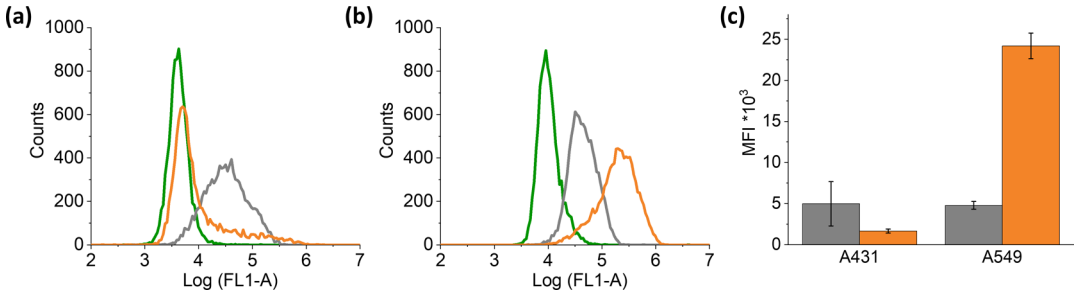

Figure 7. Flow cytometry histograms of (a) epidermal skin carcinoma cell line A431 and (b) lung cancer cell line A549 stained with the biotinylated lectins MAL **I** (α-2,3 SA) and SNA (α-2,6 SA), respectively, followed by FITC-conjugated streptavidin. (c) shows the mean fluorescence intensity (MFI) from the histograms of both cell lines. (control—green, MAL **I**—gray, SNA—orange).

https://doi.org/10.1021/acsapm.0c01353
ACS Appl. Polym. Mater. XXXX, XXX, XXX−XXX

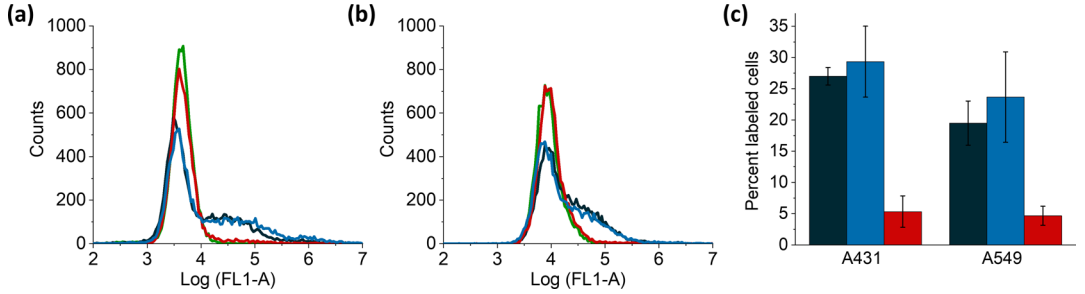

Figure 8. Flow cytometry histograms of (a) epidermal skin carcinoma cell line A431 and (b) lung cancer cell line A549 stained with 0.1 mg mL^{-1} in PBS of **MIP@SiO_2@PS**, **NIP@SiO_2@PS**, and **LA-NIP@SiO_2@PS**. (c) shows the percentage of positively labeled cells determined from the histograms of both cell lines. (Control—green, **MIP@SiO_2@PS**—black, **NIP@SiO_2@PS**—blue, **LA-NIP@SiO_2@PS**—red).

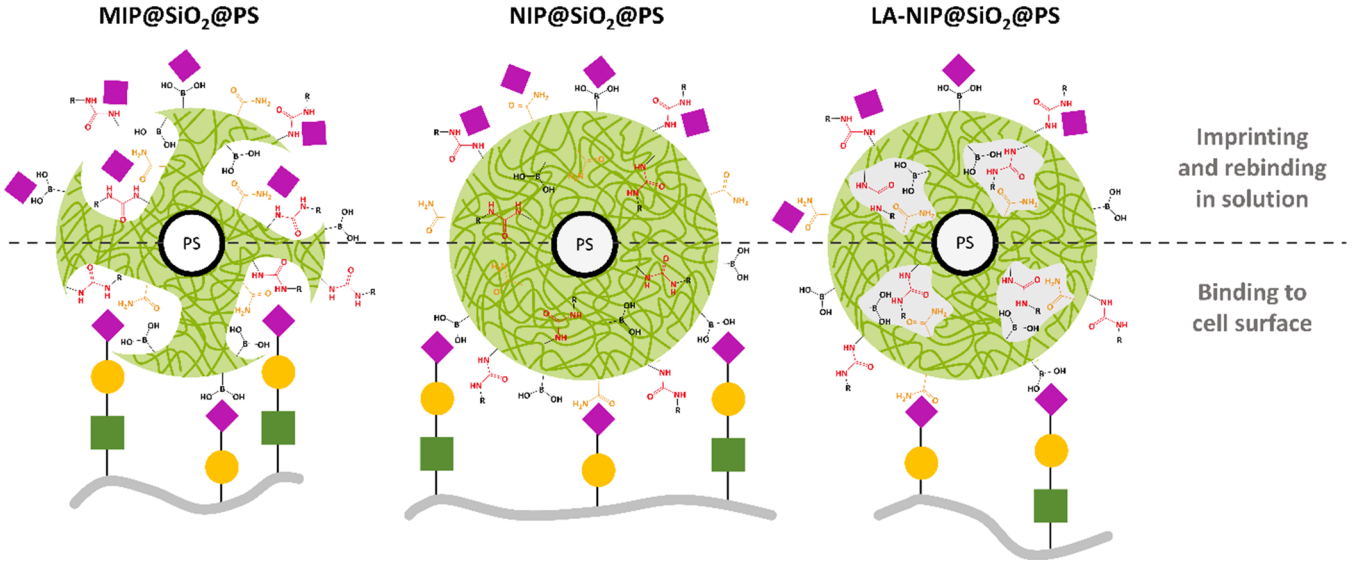

Figure 9. Schematic drawing of the proposed binding of SA (purple rhomb) to **MIP@SiO_2@PS** (left), **NIP@SiO_2@PS** (middle), and **LA-NIP@SiO_2@PS** (right) in solution and cell experiments.

binding of the particles is quantified by the fraction of cells that are fluorescently labeled since fluorescence intensity changes cannot be easily monitored for a composite object such as a micron-sized cell carrying (varying) numbers of ca. 170 nm-sized particle stains on their surface, which itself can bind to one or more SA-expressing glycan structures protruding from the cell surface. In this case, the binding behavior of the particles can be explained by the differing orientation of boronic acid groups and hydrogen bonding groups of MAAm in and on the MIP shell. During the synthesis of **MIP@SiO_2@PS** and **LA-NIP@SiO_2@PS**, cavities targeting SA and LA, respectively, are formed, in which the template-binding moieties are oriented inward in the polymer network. Hence, these groups are solely accessible to the template molecules if they fit into the formed cavity, which results in specific binding of SA on the cell surface by **MIP@SiO_2@PS** but low cell binding of **LA-NIP@SiO_2@PS**. Since the binding mode of LA to the monomers is similar to that of SA, the template binding moieties in **LA-NIP@SiO_2@PS** are enclosed in the inner regions of the polymer network creating a polymer surface profile similar to **MIP@SiO_2@PS**, but because the cavities present are not complementary to SA, only nonspecific binding is observed. Indeed, the degree of binding of **LA-NIP@SiO_2@PS** to both cell lines is the same, further confirming this hypothesis. In case of **NIP@SiO_2@PS**, no cavities are formed in the polymer network, resulting in a random arrangement of the functional groups able to interact with the template on the outer surface of the polymer network. These groups are now easily accessible by SA molecules and other polar groups on the cell surface, which will lead to a high apparent binding in cell experiments (Figure 8) but a nondetectable binding in fluorescence titrations (Figure 5). It is important to note that a rather high amount of the cross-linker was used in MIP synthesis and that the two functional and the one structural comonomer were used only in stoichiometric quantities, that is, that only when the latter are not engaged in cavity formation as in **NIP@SiO_2@PS**, they can be present to a sizeable degree on the outer surface of the polymer layer.

Zeta potential measurements at physiological pH support this assumption (Figure 10). The surface charge of **NIP@SiO_2@PS** is more positive compared to that of **MIP@SiO_2@PS** and **LA-NIP@SiO_2@PS**, which is attributed to the larger number of amide groups supplied by MAAm being exposed on the surface of **NIP@SiO_2@PS**. **LA-NIP@SiO_2@PS** is less positive, indicating the presence of fewer amide groups on the surface. **MIP@SiO_2@PS** displays the most negative potential, showing that the majority of the amide groups are within the polymer matrix, oriented within the binding cavities. This is expected since SA carries more hydroxyl groups for hydrogen bonding with MAAm compared to LA (Figure 2). With **NIP@SiO_2@PS**, the absence of template leads to a disordered arrangement of potentially template binding functional groups.

https://doi.org/10.1021/acsapm.0c01353
ACS Appl. Polym. Mater. XXXX, XXX, XXX−XXX

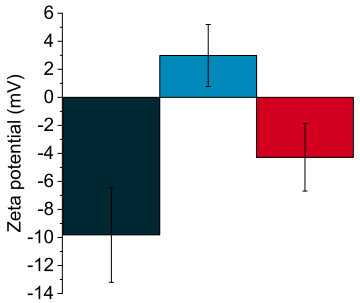

Figure 10. Zeta potential of **MIP@SiO$_2$@PS** (black), **NIP@SiO$_2$@PS** (blue), and **LA-NIP@SiO$_2$@PS** (red) at pH 7.4.

Therefore, **LA-NIP@SiO$_2$@PS** serves as a more realistic control for nonspecific binding of the particles to cells compared to **NIP@SiO$_2$@PS** due to more comparable surface properties of the particles.

CONCLUSIONS

We synthesized fluorescent MIP shells targeting SA on a silica-coated PS core, allowing for the first-time direct determination of SA in solution by fluorescence titrations in DMF, a polar solvent. The interaction mode introduced here stresses the potential that deprotonation−reprotonation mechanisms can play for traditional hydrogen bonding receptor units such as ureas in polar protic solvents when appropriately substituted, well complementing a recent approach on sensory MIPs for phospholipids.[36] Moreover, the MIP particles can be a useful tool for *in vitro* staining of cancer cells since the binding behavior compared favorably to that of SA-binding lectins, which is advantageous due to the comparable long-term stability of synthetic MIPs under ambient conditions. It was found that conventional NIPs prepared in the absence of template displayed high unspecific binding to cells due to random distribution of functional monomers on the particle surface. In contrast, NIPs prepared with a "dummy" template allowed appropriate orientation of the functional monomers within the polymer shell, leading to reduced nonspecific binding to cells. Further studies are being carried out with various cell lines to validate the performance of the MIPs in cell staining applications..

ASSOCIATED CONTENT

Supporting Information

The Supporting Information is available free of charge at https://pubs.acs.org/doi/10.1021/acsapm.0c01353.

NMR spectra of fluorescent monomer **I**; excitation and emission spectra of **I** and **I**$^-$ under study conditions; estimation of the binding constant of **I** with *N*-acetylneuraminic acid (SA); absorption spectra of MIP@SiO$_2$@PS, NIP@SiO$_2$@PS, and LA-NIP@SiO$_2$@PS after the washing step; zeta potential measurements; IR spectra of PS, SiO$_2$@PS, RAFT@SiO$_2$@PS, MIP@SiO$_2$@PS, NIP@SiO$_2$@PS, and LA-NIP@SiO$_2$@PS; absorption spectra of MIP@SiO$_2$@PS, NIP@SiO$_2$@PS, and LA-NIP@SiO$_2$@PS imprinted particles following titration with SA; kinetics of binding of MIP@SiO$_2$@PS and NIP@SiO$_2$@PS; determination of LOB, LOD, and LOQ of MIP@SiO$_2$@PS; cross-selectivity of MIP@SiO$_2$@PS; flow cytometry plots; fluorescence quantum yield (Φ_f) measurements; and uncertainty budget calculation (PDF)

AUTHOR INFORMATION

Corresponding Authors

Kornelia Gawlitza − *Chemical and Optical Sensing Division (1.9), Bundesanstalt für Materialforschung und prüfung (BAM), Berlin D-12489, Germany;* orcid.org/0000-0002-2043-4522; Email: kornelia.gawlitza@bam.de

Anette Gjörloff-Wingren − *Department of Biomedical Science and Biofilms Research Center for Biointerfaces, Malmö University, Malmö SE-20506, Sweden;* orcid.org/0000-0002-2993-0354; Email: anette.gjorloff-wingren@mau.se

Authors

Martha Kimani − *Chemical and Optical Sensing Division (1.9), Bundesanstalt für Materialforschung und prüfung (BAM), Berlin D-12489, Germany;* orcid.org/0000-0002-1292-9795

Sarah Beyer − *Department of Biomedical Science and Biofilms Research Center for Biointerfaces, Malmö University, Malmö SE-20506, Sweden;* orcid.org/0000-0001-8021-9624

Zahra El-Schich − *Department of Biomedical Science and Biofilms Research Center for Biointerfaces, Malmö University, Malmö SE-20506, Sweden;* orcid.org/0000-0002-0841-5804

Knut Rurack − *Chemical and Optical Sensing Division (1.9), Bundesanstalt für Materialforschung und prüfung (BAM), Berlin D-12489, Germany;* orcid.org/0000-0002-5589-5548

Complete contact information is available at: https://pubs.acs.org/10.1021/acsapm.0c01353

Author Contributions

M.K. and S.B. contributed equally to this manuscript. The manuscript was written through contributions of all authors. All authors have given approval to the final version of the manuscript.

Notes

The authors declare no competing financial interest.

ACKNOWLEDGMENTS

We thank E. Kislenko (BAM) for supplying fluorescent probe **I**, K. Keil (BAM) for performing pK_a measurements of **I**, A. Meckelburg (BAM) for performing elemental analysis, A. Kohl (BAM) for performing IR measurements, and Y. Zhang (MU) for performing cell-based MIP experiments. This research was funded by The European Union's Horizon 2020 research and innovation program under the Marie Sklodowska-Curie grant agreement grant number 721297, the Swedish Knowledge Foundation grant number 20160165, the Royal Physiographic Society of Lund, the Malmö Cancer Center, Biofilms Research Center for Biointerfaces, and Malmö University.

REFERENCES

(1) Gabius, H.-J. Glycans: bioactive signals decoded by lectins. *Biochem. Soc. Trans.* **2008**, *36*, 1491−1496.
(2) Varki, A. Biological roles of glycans. *Glycobiology* **2016**, *27*, 3−49.
(3) Dube, D. H.; Bertozzi, C. R. Glycans in cancer and inflammation - potential for therapeutics and diagnostics. *Nat. Rev. Drug Discovery* **2005**, *4*, 477−488.
(4) Adamczyk, B.; Tharmalingam, T.; Rudd, P. M. Glycans as cancer biomarkers. *Biochim. Biophys. Acta, Gen. Subj.* **2012**, *1820*, 1347−1353.

(5) Kugimiya, A.; Matsui, J.; Takeuchi, T.; Yano, K.; Muguruma, H.; Elgersma, A. V.; Karube, I. Recognition of Sialic Acid Using Molecularly Imprinted Polymer. *Anal. Lett.* **1995**, *28*, 2317−2323.
(6) Piletsky, S. A.; Piletskaya, E. V.; Yano, K.; Kugimiya, A.; Elgersma, A. V.; Levi, R.; Kahlow, U.; Takeuchi, T.; Karube, I.; Panasyuk, T. I.; El'skaya, A. V. A Biomimetic Receptor System for Sialic Acid Based on Molecular Imprinting. *Anal. Lett.* **1996**, *29*, 157−170.
(7) Kugimiya, A.; Yoneyama, H.; Takeuchi, T. Sialic Acid Imprinted Polymer-Coated Quartz Crystal Microbalance. *Electroanalysis* **2000**, *12*, 1322−1326.
(8) Otsuka, H.; Uchimura, E.; Koshino, H.; Okano, T.; Kataoka, K. Anomalous Binding Profile of Phenylboronic Acid with N-Acetylneuraminic Acid (Neu5Ac) in Aqueous Solution with Varying pH. *J. Am. Chem. Soc.* **2003**, *125*, 3493−3502.
(9) Panagiotopoulou, M.; Kunath, S.; Medina-Rangel, P. X.; Haupt, K.; Tse Sum Bui, B. Fluorescent molecularly imprinted polymers as plastic antibodies for selective labeling and imaging of hyaluronan and sialic acid on fixed and living cells. *Biosens. Bioelectron.* **2017**, *88*, 85−93.
(10) Liu, R.; Cui, Q.; Wang, C.; Wang, X.; Yang, Y.; Li, L. Preparation of Sialic Acid-Imprinted Fluorescent Conjugated Nanoparticles and Their Application for Targeted Cancer Cell Imaging. *ACS Appl. Mater. Interfaces* **2017**, *9*, 3006−3015.
(11) Luo, Y.; Yang, Y.; Cui, Q.; Peng, R.; Liu, R.; Cao, Q.; Li, L. Fluorescent Nanoparticles Synthesized by Carbon-Nitride-Stabilized Pickering Emulsion Polymerization for Targeted Cancer Cell Imaging. *ACS Appl. Bio Mater.* **2019**, *2*, 5127−5135.
(12) Wang, S.; Yin, D.; Wang, W.; Shen, X.; Zhu, J.-J.; Chen, H.-Y.; Liu, Z. Targeting and Imaging of Cancer Cells via Monosaccharide-Imprinted Fluorescent Nanoparticles. *Sci. Rep.* **2016**, *6*, 22757.
(13) Shinde, S.; El-Schich, Z.; Malakpour, A.; Wan, W.; Dizeyi, N.; Mohammadi, R.; Rurack, K.; Gjörloff Wingren, A.; Sellergren, B. Sialic Acid-Imprinted Fluorescent Core-Shell Particles for Selective Labeling of Cell Surface Glycans. *J. Am. Chem. Soc.* **2015**, *137*, 13908−13912.
(14) El-Schich, Z.; Abdullah, M.; Shinde, S.; Dizeyi, N.; Rosén, A.; Sellergren, B.; Wingren, A. G. Different expression levels of glycans on leukemic cells-a novel screening method with molecularly imprinted polymers (MIP) targeting sialic acid. *Tumor Biol.* **2016**, *37*, 13763−13768.
(15) Sarma, D.; Gawlitza, K.; Rurack, K. Polystyrene Core-Silica Shell Particles with Defined Nanoarchitectures as a Versatile Platform for Suspension Array Technology. *Langmuir* **2016**, *32*, 3717−3727.
(16) Sarma, D.; Carl, P.; Climent, E.; Schneider, R. J.; Rurack, K. Multifunctional Polystyrene Core/Silica Shell Microparticles with Antifouling Properties for Bead-Based Multiplexed and Quantitative Analysis. *ACS Appl. Mater. Interfaces* **2019**, *11*, 1321−1334.
(17) Wan, W.; Biyikal, M.; Wagner, R.; Sellergren, B.; Rurack, K. Fluorescent Sensory Microparticles that "Light-up" Consisting of a Silica Core and a Molecularly Imprinted Polymer (MIP) Shell. *Angew. Chem., Int. Ed.* **2013**, *52*, 7023−7027.
(18) Maus, M.; Rurack, K. Monitoring pH and solvent proticity with donor-acceptor-substituted biphenyls: a new approach towards highly sensitive and powerful fluorescent probes by tuning the molecular structure. *New J. Chem.* **2000**, *24*, 677−686.
(19) Nandiyanto, A. B. D.; Suhendi, A.; Ogi, T.; Iwaki, T.; Okuyama, K. Synthesis of additive-free cationic polystyrene particles with controllable size for hollow template applications. *Colloids Surf., A* **2012**, *396*, 96−105.
(20) Nandiyanto, A. B. D.; Akane, Y.; Ogi, T.; Okuyama, K. Mesopore-Free Hollow Silica Particles with Controllable Diameter and Shell Thickness via Additive-Free Synthesis. *Langmuir* **2012**, *28*, 8616−8624.
(21) Wagner, S.; Bell, J.; Biyikal, M.; Gawlitza, K.; Rurack, K. Integrating fluorescent molecularly imprinted polymer (MIP) sensor particles with a modular microfluidic platform for nanomolar small-molecule detection directly in aqueous samples. *Biosens. Bioelectron.* **2018**, *99*, 244−250.
(22) Schneider, C. A.; Rasband, W. S.; Eliceiri, K. W. NIH Image to ImageJ: 25 years of image analysis. *Nat. Methods* **2012**, *9*, 671−675.
(23) Wagner, S.; Zapata, C.; Wan, W.; Gawlitza, K.; Weber, M.; Rurack, K. Role of Counterions in Molecularly Imprinted Polymers for Anionic Species. *Langmuir* **2018**, *34*, 6963−6975.
(24) Kolthoff, I. M.; Chantooni, M. K.; Smagowski, H. Acid-base strength in N,N-dimethylformamide. *Anal. Chem.* **1970**, *42*, 1622−1628.
(25) Maran, F.; Celadon, D.; Severin, M. G.; Vianello, E. Electrochemical determination of the pKa of weak acids in N,N-dimethylformamide. *J. Am. Chem. Soc.* **1991**, *113*, 9320−9329.
(26) Brynn Hibbert, D.; Thordarson, P. The death of the Job plot, transparency, open science and online tools, uncertainty estimation methods and other developments in supramolecular chemistry data analysis. *Chem. Commun.* **2016**, *52*, 12792−12805.
(27) Nishitani, S.; Maekawa, Y.; Sakata, T. Understanding the Molecular Structure of the Sialic Acid-Phenylboronic Acid Complex by using a Combined NMR Spectroscopy and DFT Study: Toward Sialic Acid Detection at Cell Membranes. *ChemistryOpen* **2018**, *7*, 513−519.
(28) Sellergren, B.; Hall, A. J., Chapter 2 - Fundamental aspects on the synthesis and characterisation of imprinted network polymers. In *Techniques and Instrumentation in Analytical Chemistry*; Sellergren, B., Ed.; Elsevier, 2001; Vol. *23*, pp 21−57.
(29) Sartain, F. K.; Yang, X.; Lowe, C. R. Complexation of L-Lactate with Boronic Acids: A Solution and Holographic Analysis. *Chem. - Eur. J.* **2008**, *14*, 4060−4067.
(30) Lusi, E.; Ratna, B.; Takashi, O.; Kikuo, O.; Tomonori, T. Role of Acetone in the Formation of Highly Dispersed Cationic Polystyrene Nanoparticles. *Chem. Eng. Process.* **2017**, *38*, 5−18.
(31) Wan, W.; Descalzo, A. B.; Shinde, S.; Weißhoff, H.; Orellana, G.; Sellergren, B.; Rurack, K. Ratiometric Fluorescence Detection of Phosphorylated Amino Acids Through Excited-State Proton Transfer by Using Molecularly Imprinted Polymer (MIP) Recognition Nanolayers. *Chem.—Eur. J.* **2017**, *23*, 15974−15983.
(32) Oztürk, L. K.; Emekli-Alturfan, E.; Kasikci, E.; Demir, G.; Yarat, A. Salivary total sialic acid levels increase in breast cancer patients: a preliminary study. *Med. Chem.* **2011**, *7*, 443−447.
(33) Hernández-Arteaga, A.; de Jesús Zermeño Nava, J.; Kolosovas-Machuca, E. S.; Velázquez-Salazar, J. J.; Vinogradova, E.; José-Yacamán, M.; Navarro-Contreras, H. R. Diagnosis of breast cancer by analysis of sialic acid concentrations in human saliva by surface-enhanced Raman spectroscopy of silver nanoparticles. *Nano Res.* **2017**, *10*, 3662−3670.
(34) Ulloa, F.; Real, F. X. Differential Distribution of Sialic Acid in α2,3 and α2,6 Linkages in the Apical Membrane of Cultured Epithelial Cells and Tissues. *J. Histochem. Cytochem.* **2001**, *49*, 501−509.
(35) Hui, C. F.; Chan, R. W.; Fung, K.; Yu, W. C.; Tsao, S.; Chan, M. C.; Nicholls, J. M. The regional distribution of different types of influenza receptors in cultured human alveolar epithelial cells and correlation with in vitro infection. *Influenza Other Respir. Viruses* **2011**, *5*, 436−437.
(36) Li, Q. J.; Shinde, S.; Grasso, G.; Caroli, A.; Abouhany, R.; Lanzillotta, M.; Pan, G. Q.; Wan, W.; Rurack, K.; Sellergren, B. Selective detection of phospholipids using molecularly imprinted fluorescent sensory core-shell particles. *Sci. Rep.* **2020**, *10*, 9924.

https://doi.org/10.1021/acsapm.0c01353
ACS Appl. Polym. Mater. XXXX, XXX, XXX−XXX